



Cite this: *Nanoscale*, 2016, 8, 1133

## Thermal curing of a self-assembled monolayer at the nanoscale†

Zhengqing Zhang,<sup>a</sup> Hyojeong Kim,<sup>a</sup> Jaegeun Noh,<sup>b</sup> Yoonho Ahn,<sup>c</sup> Jong Yeog Son<sup>c</sup> and Joonkyung Jang\*<sup>a</sup>

On fabrication by contact printing, a nanostructured self-assembled monolayer (SAM) of alkanethiol contains a substantial fraction of unbound molecules that are either inverted among other upright molecules or piled on top of the SAM. The molecular dynamics simulation in the present study demonstrates that thermal annealing cures these defects for a SAM island of octadecanethiol. The SAM island melted partially as a result of heating, so the unbound molecules that had piled on top of the SAM island penetrated down to make contact with the surface, and the inverted molecules flipped to achieve adsorption. With subsequent cooling, the packing of sulfur atoms and alignment of alkyl chains of the SAM island were recovered. The molecular pathways for the adsorption of the unbound molecules were unraveled. The transition state and activation energy, calculated for each pathway in the absence of annealing, showed that these defects are incurable without the help of annealing.

Received 23rd September 2015,  
Accepted 2nd December 2015

DOI: 10.1039/c5nr06559c

www.rsc.org/nanoscale

### Introduction

Nanostructured self-assembled monolayers (SAMs) of alkanethiols are utilized in various applications, such as functional nanomaterials,<sup>1–3</sup> biosensors,<sup>4</sup> and molecular electronics.<sup>5–7</sup> All of these applications are based on the notion that the nanoscale SAMs have the same ordered and stable structure as the bulk SAMs at full surface coverage: the sulfur atoms are closely packed with each other and firmly bound to the surface, and the alkyl chains are aligned and packed together.<sup>8,9</sup> Nanosized SAMs, however, exhibit some novel features: for example, the tilt orientation of the alkyl chains periodically changes with time and the SAMs become unstable when their sizes fall below certain values (5 nm and 3 nm in width for the SAM dots and lines, respectively).<sup>10–12</sup> At present, the molecular and thermal properties of nanoscale SAMs are poorly understood, compared to their bulk counterparts.

A nanostructured SAM is often fabricated by contact printing utilizing a source with nano- or microscale asperities such as a stamp<sup>9</sup> or an atomic force microscope (AFM) tip<sup>13</sup> coated with thiol molecules. Essential in this nano- or microcontact

printing is the self-assembly of a multi-layered mound of entangled molecules into an ordered monolayer.

Owing to the largely random nature of molecular tumbling and diffusion in the self-assembly, however, the resulting SAM pattern inevitably includes a significant amount of unbound thiol molecules, as shown in Fig. 1 (nearly 20% for the present simulation of a SAM island). These unbound thiol molecules were detected in the X-ray photoelectron spectra of the bulk SAMs.<sup>14–16</sup> For example, the minor sulfur peak for the SAM of L-cysteine was attributed to the molecules physisorbed on the first chemisorbed layer.<sup>16</sup> However, spectroscopic or micro-

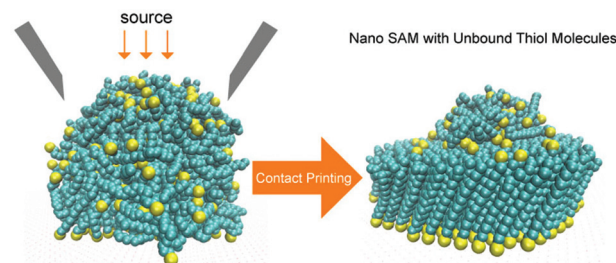


**Fig. 1** A circular SAM island of ODT (7 nm in diameter) fabricated by contact printing. A mound of entangled ODT molecules (left), deposited by contact printing, spreads and self-assembles into a SAM island containing unbound molecules either inverted among upright molecules or piled on top of the SAM island. Spreading of an entangled mound of thiol molecules into a monolayer is an essential step in nano- or micro-contact printing of SAMs. In this and all of the following figures, the underlying surface is gold (111) and is drawn as dots.

<sup>a</sup>Department of Nanoenergy Engineering, Pusan National University, Busan 609-735, South Korea. E-mail: jkjang@pusan.ac.kr

<sup>b</sup>Department of Chemistry and Institute of Nano Science and Technology, Hanyang University, Seoul 133-791, South Korea

<sup>c</sup>Department of Applied Physics, Kyung Hee University, Yongin 446-701, South Korea

†Electronic supplementary information (ESI) available. See DOI: 10.1039/c5nr06559c

scopic probing of the unbound thiol molecules of a nanoscale SAM has been elusive. Instead, a molecular dynamics (MD) simulation can provide a detailed picture of the unbound thiol molecules.<sup>12</sup> In addition to the molecules piled on top of the SAM through nonspecific van der Waals interactions, our previous MD simulation has revealed the existence of inverted molecules among upright molecules whose methyl tail groups, instead of sulfur atoms, make contact with the surface.

The unbound molecules of nanoscale SAMs can seriously limit their stabilities and efficiencies in various applications, such as sensors, nanomolding, and nanoreplication. Here, we propose thermal annealing as an efficient cure for these defects. Thermal annealing is known to reduce the number of disordered domains of the bulk SAM<sup>17–19</sup> by decreasing the amount of vacancy islands (pits) of the underlying surface. Even on an atomically flat surface such as a gold (111) surface, however, a SAM can have defects such as pinholes due to the alkyl chains not being fully extended and the domain boundaries arising from the mismatch in the tilt direction of alkyl chains.<sup>12,20,21</sup> Nanostructured SAMs, having the novel structural features described above, are presumably more vulnerable to thermal fluctuation compared to their bulk counterparts.<sup>10,11</sup> Currently, the effects of thermal annealing on nanostructured SAMs are unknown.

Herein, MD simulation was used to study thermal annealing (400 K) of the SAM island of 1-octadecanethiol (ODT) with unbound thiol molecules. These unbound molecules are relevant to those resulting naturally from the nanocontact printing of a circular SAM pattern. We show that thermal annealing effectively cures the unbound molecules in the SAM island, giving rise to an ordered and compact SAM island. We resolved the molecular pathways for the adsorption of unbound molecules in the annealing process. We identified the transition states and calculated the activation energies for these pathways. Our investigation shows that the unbound molecules of the present SAM island cannot be cured without the help of thermal annealing.

## Results and discussion

A circular SAM island of ODT, 7 nm in diameter, was grown on a gold (111) surface by nanocontact printing (Fig. 1). The contact printing was emulated by spreading a droplet of ODT molecules on the surface. The mound of entangled molecules (left, Fig. 1) spread spontaneously and self-assembled into a SAM island with unbound molecules either inverted among upright molecules or piled on top of the SAM island. These unbound molecules, arising from the random molecular tumbling and diffusion in the self-assembly, accounted for 20% of the 346 total molecules comprising the SAM island (11% inverted and 9% piled on top of the SAM island). Presumably, these unbound molecules are ubiquitous in the nanosized SAMs grown by contact printing. However, the thermal properties of these unbound molecules, especially those inverted, were previously unexplored.

The SAM island grown by nanocontact printing (right, Fig. 1) was subsequently annealed at 400 K (Fig. 2). Upon heating from 300 to 400 K, the SAM island melted partially without desorption of molecules; it expanded laterally, and the sulfur atoms, which were initially closely packed, dispersed slightly. At the same time, the alkyl chains became curly and disordered, in contrast to the initially straight alkyl chains that were aligned with each other. At 380 K, all of the molecules that piled on top of the SAM island penetrated down to make contact with the surface, either upright or inverted. When the temperature reached 400 K, all of the inverted molecules flipped to stand upright. Upon subsequent cooling to 300 K, the sulfur atoms were densely packed again, giving the  $\sqrt{3} \times \sqrt{3}R30^\circ$  overlayer packing of sulfur atoms. Moreover, the alkyl chains aligned with each other, resulting in a nearly defect-free compact SAM island. The structural parameters of the SAM island after the completion of annealing were examined (see Table S1, ESI†).<sup>12</sup> The sulfur–sulfur distance (4.97 Å), tilt angle of alkyl chains (26.1°), percentage of *trans* conformations of alkyl chains (97.1%), and order parameter of the tilt orientation of alkyl chains were all close to the corresponding values of the bulk SAMs without any defects.

Two pinholes remained in the SAM island after the completion of annealing because two molecules folded their alkyl chains in half, blocking two adsorption sites on the surface.

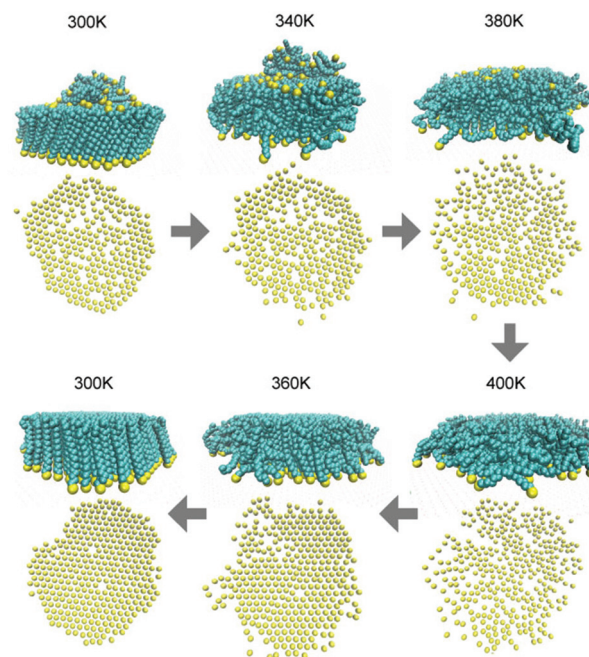


**Fig. 2** Thermal annealing of the present SAM island initially containing unbound molecules. Selected snapshots of the SAM island in the annealing arranged sequentially in the clockwise direction (starting from the top left panel) are shown. In each panel, the bottom view of the sulfur atoms of the SAM island is also shown. The temperature was increased (decreased) by 20 K. At each temperature, MD simulation was run for 4 ns.

Interestingly, similar pinholes were found in the AFM images of the crystalline domains of the bulk SAMs and were attributed to alkyl chains that were not fully extended.<sup>20</sup> Note that the present SAM island was annealed extremely fast (at a rate of  $4.2 \text{ K ns}^{-1}$ ), owing to the limited timescale of MD simulation (which lasts only up to the sub-microsecond scale). An experimental annealing, done much more slowly, will give a more ordered SAM structure, presumably without the pinholes seen above. We examined the structures of the SAM islands annealed two and four times faster than in the present simulation (Table S1, ESI†). We observed a clear trend that a slower annealing gives rise to a reduced number of pinholes and an enhanced orientational order in the alkyl chains of the SAM island. Similarly, the previous experiments showed that a reduced annealing rate decreases the number of defects (and increases the range of ordered domains) in the bulk SAMs.<sup>22,23</sup>

We were able to identify four molecular pathways for the adsorption of the unbound molecules in the annealing process (Fig. 3). The unbound molecules piled on top of the SAM island (46% of the 70 total unbound molecules) followed the hop-down (44%) or push-down (56%) adsorption pathway. In the hop-down pathway, a molecule migrated to the SAM periphery and hopped down to the bare surface. In the push-down pathway, a molecule that was stacked on top of the SAM

island pushed away the molecules below it and made contact with the surface. The molecules that had been pushed away in turn pushed their neighbors, and these pushing events propagated toward the SAM periphery. Before the temperature reached 400 K, the pile of molecules on top of the SAM island disappeared completely (more details can be found in Fig. S1, ESI†). The present hop-down and push-down pathways are similar to those found in our MD simulation of the growth of a SAM island by contact printing.<sup>12</sup>

The adsorption of an inverted thiol molecule in the annealing process followed either a sequential (18%) or simultaneous (82%) flip pathway (Fig. 3). In the former case, the sulfur atom of an inverted molecule pushed its way down to the surface without moving its methyl tail group. Only after the sulfur atom adsorbed, the methyl tail group went up, resulting in an upright adsorbed molecule. In the latter, the sulfur atom of an inverted molecule went down to the surface and adsorbed to the surface while simultaneously raising its methyl tail group above it. Consecutive snapshots of the sequential and simultaneous flip pathways can be found in Fig. S2, ESI.†

The question that arises at this point is whether the unbound molecules spontaneously adsorb without thermal annealing over a long timescale relevant to the experiment (hours or days). As MD simulation over an experimental timescale is not possible, we instead calculated the activation energy required for a molecule to adsorb by following each pathway above without annealing. To do so, the free energy profile for each pathway was constructed by running a series of restrained MD simulations at 300 K (see the Simulation methods section for details).

The free energy or potential of mean force (PMF) for the hop-down pathway was calculated by varying the horizontal position of the sulfur atom of an unbound molecule,  $\varphi$  (Fig. 4). As  $\varphi$  increased from 0 to  $38.5 \text{ \AA}$  (from the center to the periphery of the SAM island), the maximum free energy (transition state) appeared at  $\varphi = 37.2 \text{ \AA}$  with a barrier height of 4.0 times the thermal energy at 300 K,  $k_{\text{B}}T$ . The snapshot of the transition state (marked as a circle in the PMF curve) is shown in Fig. 4. This barrier is similar to the Ehrlich-Schwoebel (ES) barrier originally defined as the extra energy required for an adatom to step down at the step edge in the epitaxial growth of a metal film.<sup>24,25</sup> The ES barrier arises from the reduced number of neighbors of an adatom at the step edge compared to that of an adatom on top of a terrace. Note, however, that the present adsorbing molecule (in red) dragged the pile of molecules from the center to the periphery of the SAM island. Therefore, the present barrier contains, in addition to the ES barrier, the energy required to detach the adsorbing molecule from the pile of molecules stacked on top of the SAM island. The ES barrier for the present SAM island can be calculated by removing the pile of molecules on top of the SAM island except the adsorbing molecule. In this way, the ES barrier of the present SAM island was found to be  $0.7k_{\text{B}}T$  (see Fig. S3, ESI†). The present ES barrier is much smaller than that calculated for an organic transistor film of tetracene,  $\sim 7.8k_{\text{B}}T$ , even though tetracene is similar to ODT in mass.<sup>26</sup> This presumably

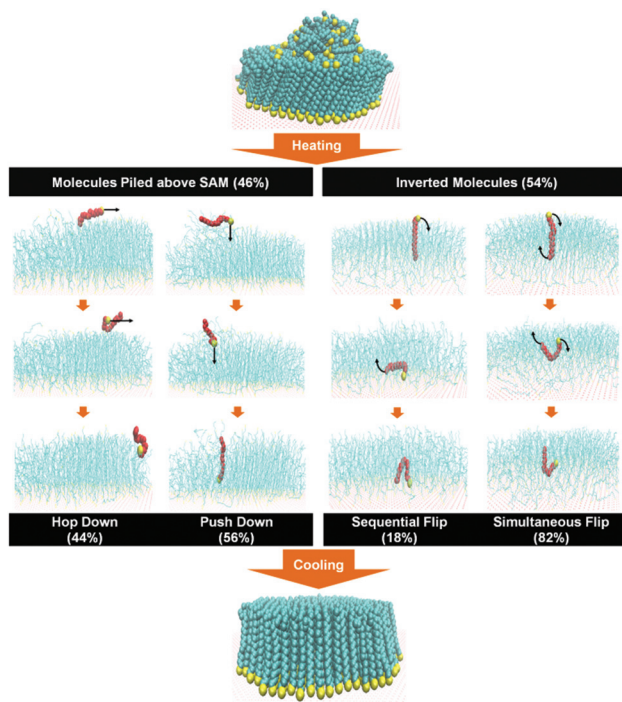


**Fig. 3** Molecular pathways for the adsorption of unbound molecules in the present annealing. Two types of unbound molecules, either inverted among other upright molecules (54%) or piled on top of the SAM island (46%), were found. An unbound molecule piled on top of the SAM island followed either a hop-down (44%) or push-down (56%) pathway to achieve adsorption. An inverted molecule followed either a simultaneous (82%) or sequential (18%) flip pathway to achieve adsorption.

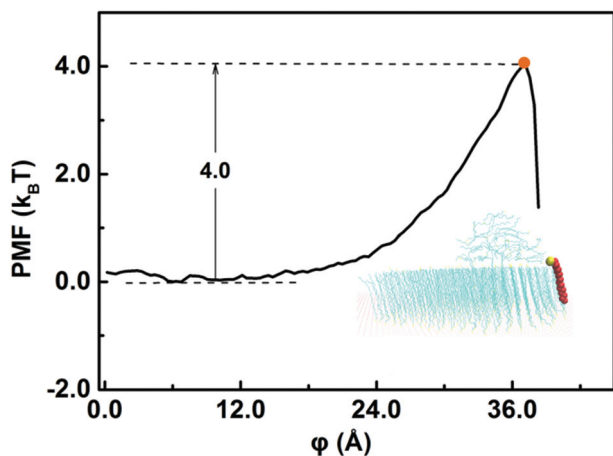


Fig. 4 Free energy profile for the adsorption of an ODT molecule through the hop-down pathway without annealing. The PMF was calculated by varying the lateral position of the sulfur atom measured from the center of the SAM island,  $\phi$ , from 0 to 38.5 Å. Also shown is the configuration of the transition state with the maximal free energy (marked as a circle). In this and all of the following figures, the PMF values are reported in units of thermal energy at 300 K,  $k_B T$  (2.49 kJ mol<sup>-1</sup>). Moreover, ODT molecules, except for the adsorbing one, are depicted as lines.

arises from the fact that ODT molecules are floppy and weakly bound together, in contrast to rigid tetracene molecules strongly bound together through  $\pi$ - $\pi$  stacking interaction. In this and all of the following PMF profiles, the focus is on the transition state and activation energy of an adsorbing molecule. The PMF values at geometries near adsorption (when the sulfur atom is close to a gold atom) were omitted, because the strong chemisorption interaction makes it difficult to control the position of the sulfur atom in the restrained MD simulation (see the Simulation methods section for details).

The PMF profile of a molecule adsorbing through the push-down pathway without annealing is shown in Fig. 5. Here, the height of the sulfur atom measured from the gold surface,  $\xi$ , was controlled in the restrained MD simulation. The MD snapshots of two transition states (marked as circles) are shown as well. Upon lowering the sulfur atom (decreasing  $\xi$  from 23.4 to 4.4 Å), two free energy barriers are met. After crossing the first small barrier of  $5.3k_B T$  in height, a local minimum appeared when the sulfur atom was halfway down to the surface ( $\xi = 15.5$  Å). As the sulfur atom was lowered further, the maximum free energy emerged at  $\xi = 6.6$  Å with a barrier height of  $18.8k_B T$ . Here, more energy is required to push away the sulfur atoms already bound to the surface. The free energy barriers above ( $>18k_B T$ ) signify that the molecular adsorption following the push-down pathway is implausible in the absence of annealing.

The PMF profile of the molecular adsorption *via* the sequential flip pathway consisted of two steps (Fig. 6). In the first step, the sulfur atom of an adsorbing molecule pushed its way down without moving its methyl tail group. The PMF curve calculated by controlling  $\xi$  is displayed in Fig. 6 (top),

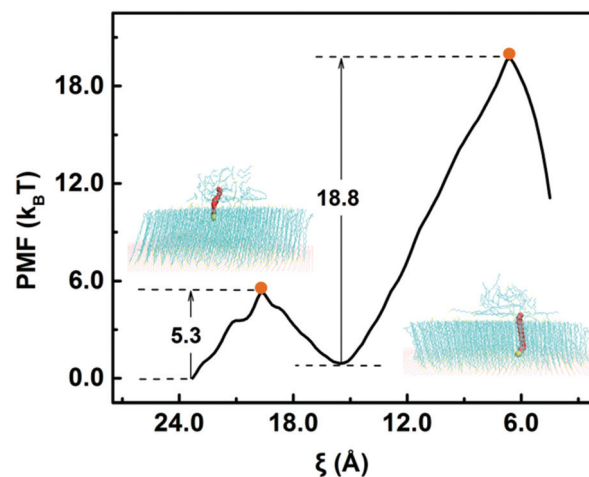
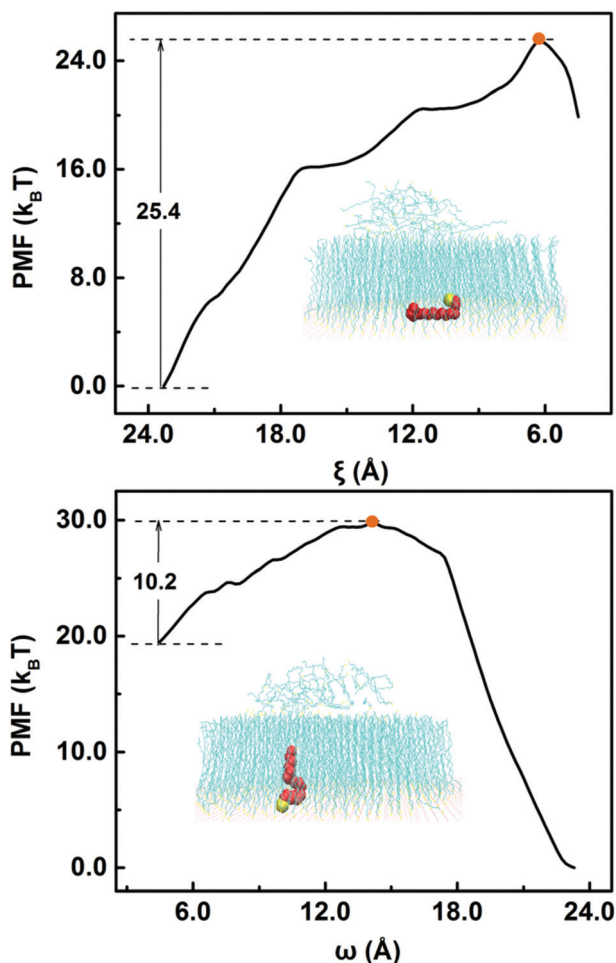


Fig. 5 Free energy profile for a molecule adsorbing through the push-down pathway without annealing. The PMF curve was constructed by controlling the height of the sulfur atom measured from the gold surface,  $\xi$ . Also depicted are the simulation snapshots for the transition states with the free energy maxima, marked as circles.

along with the snapshot of the transition state (marked as a circle). As  $\xi$  decreased from 23.4 to 4.4 Å, the PMF increased, reaching a maximum with a height of  $25.4k_B T$  at  $\xi = 6.2$  Å, followed by a decrease. This barrier is even larger than that found for the push-down pathway. In the second step, the methyl tail group rose while the sulfur atom was tethered to the surface. Fig. 6 (bottom) shows the PMF plotted against the vertical height of the terminal methyl group,  $\omega$ . The MD snapshot of the transition state (circled) is shown. As  $\omega$  increased from 4.4 to 23.4 Å, the free energy increased, reaching a maximum at  $\omega = 14.8$  Å, followed by a decrease. Here, the free energy barrier is  $\sim 10k_B T$ , indicating that the methyl tail group rises more easily than the sulfur atom penetrates down.

Lastly, the PMF profile for a molecule adsorbing *via* the simultaneous flip pathway without annealing was investigated (Fig. 7). Because the sulfur atom and methyl tail group moved simultaneously down and up, respectively, the PMF was plotted against both  $\xi$  and  $\omega$ , by varying  $\xi$  from 23.4 to 4.4 Å and  $\omega$  from 4.4 to 23.4 Å. Only the diagonal portion of the PMF surface was calculated because  $\xi$  and  $\omega$  vary simultaneously in the opposite direction. Also shown is the MD snapshot of the transition state (marked as a cross) located at  $(\xi, \omega) = (12.1 \text{ Å}, 16.9 \text{ Å})$ . The free energy barrier was  $28k_B T$  in height, several  $k_B T$  values higher than that found in the sequential flip pathway.

As seen above, the adsorption of an unbound molecule, whether it was inverted among upright molecules or piled on top of the SAM island, requires an activation energy much larger than the thermal energy at room temperature. Moreover, the push-down and sequential flip pathways had double barriers, leading to intermediate metastable states. The activation energy of the hop-down pathway was relatively small but still four times the thermal energy. Moreover, the adsorbing molecule in this case must diffuse from the center to the periphery



**Fig. 6** Free energy profile for the adsorption of a molecule *via* the sequential flip pathway in the absence of annealing. This pathway consisted of two steps. First, the sulfur atom penetrated down without moving the methyl tail group. The plot of PMF against the height of the sulfur atom,  $\xi$  (top), is shown, along with the snapshot of the transition state (marked as a circle). The second step involves the raising of the methyl tail group while the sulfur atom is tethered to the surface. The plot of PMF against the height of the methyl tail  $\omega$  (bottom) is shown, together with the MD snapshot of the transition state (marked as a circle).

of the SAM island. This should require additional time, particularly for a large SAM island, making adsorption through the hop-down pathway even more implausible. Consequently, the unbound molecules in the present SAM island are incurable without thermal annealing.

We point out that the present MD method has proven to capture the experimental features of the bulk SAM. For example, the equilibrium SAM structures such as the tilt angles of alkyl chains and the hexagonal packing of sulfur atoms were in good agreement with the experimental results.<sup>27,28</sup> Unfortunately however, we are unaware of any experimental investigation on the structure of a nanoscale SAM due to the inherent difficulty in probing small SAMs. Moreover, the present study focused on the mechanism and

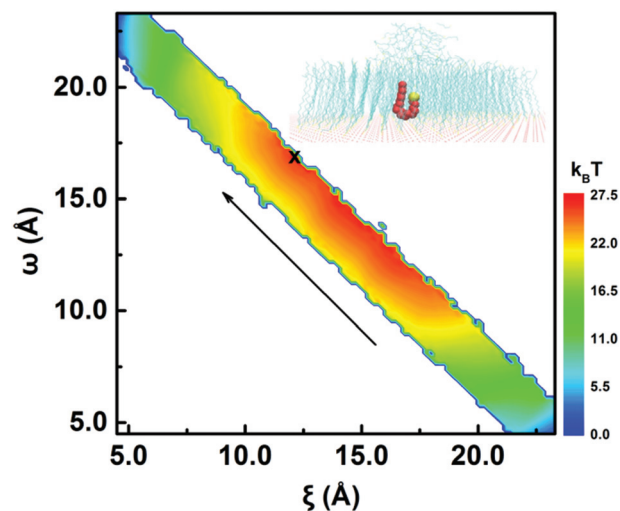


**Fig. 7** Free energy profile for the adsorption of an unbound molecule *via* the simultaneous flip pathway in the absence of annealing. The plot of PMF against both  $\xi$  and  $\omega$  is shown, with the MD snapshot of the transition state (marked as a cross). The arrow shows the direction of progress in the adsorption.

transition states of curing of the nanoscale SAM, making a direct comparison with the experiment even more elusive.

We selected a rather long alkanethiol molecule because ODT is a prototypical molecule in the nanofabrication of SAM.<sup>29</sup> Thermal curing found for the SAM of ODT is expected to be valid for alkanethiols with different chain lengths (typically varying from 8 to 30 in the number of carbon atoms). Quantitatively however, the SAMs of alkanethiol molecules with relatively short chain lengths will be cured even more rapidly by thermal annealing. The reason is twofold. First, the unbound molecules on top of the SAM island diffuse faster, and, consequently, more rapidly adsorb to the surface *via* the hop-down pathway. Second, the inverted molecules with short chain lengths will flip relatively easily to adsorb *via* the flip mechanisms. If the alkyl chains are too short however (less than 10 carbon atoms), a nanoscale SAM will be thermally unstable due to its weak interchain packing, as found previously.<sup>30–32</sup>

The final state of the present SAM island does depend on the initial positions and velocities of the alkanethiol molecules used in MD simulations. Therefore, the final structure of SAM, such as the exact shape of the periphery of SAM, can be slightly different, depending on the initial conditions used. However, thermal annealing will invariably remove the unbound molecules regardless of the initial conditions, because the free energy barriers for the adsorption of unbound molecules are removed by thermal annealing.

### Simulation methods

The  $\text{CH}_3$ ,  $\text{CH}_2$ , and  $\text{SH}$  groups of ODT were treated as united atoms,<sup>33,34</sup> because this united atom model previously

produced SAM structures that were in agreement with the all-atom simulations.<sup>35,36</sup> The bond stretching and bending angle interactions were modeled as harmonic potentials.<sup>37</sup> The four-atom torsion potential (C–C–C–C or C–C–C–S) was a triple cosine function of the dihedral angle, which has minima corresponding to the *trans* and *gauche* conformations.<sup>38</sup> Non-bonded interatomic interactions were described using the Lennard-Jones (LJ) potentials,

$$V_{\text{LJ}}(r) = 4\varepsilon[(\sigma/r)^{12} - (\sigma/r)^6]$$

where  $r$  is the interatomic distance, and  $\varepsilon$  and  $\sigma$  are the energy and length parameters, respectively.<sup>33</sup> The Lorentz–Berthelot combination rule<sup>39</sup> was used to obtain the LJ parameters of the heteroatomic pairs. The sulfur–gold chemisorption interaction was described by the Morse potential,<sup>40</sup>

$$V_{\text{Morse}}(r) = D e^{-\alpha(r-b)} [e^{-\alpha(r-b)} - 2]$$

where  $D$  and  $b$  are the well depth and distance at the minimum potential energy, respectively. The LJ and Morse parameters were taken from previous studies.<sup>10,12,27,33</sup> The gold (111) surface was made of two layers of 12 800 atoms and held rigid. We simulated the largest gold surface as possible to mimic a surface relevant to experiments. The MD trajectories were propagated using the velocity Verlet algorithm with a time step of 1.0 fs.

A spherical droplet of 346 ODT molecules was simulated by running a constant number, volume, and temperature (NVT) MD simulation at 300 K for 2 ns using the Berendsen thermostat.<sup>41</sup> The droplet was then placed 1.0 nm above the gold surface. An NVT MD simulation was then run for 79.92 ns, and the final configuration was used as the initial condition for the annealing simulation (right, Fig. 1). The initial SAM island with unbound molecules was heated to 400 K in increments of 20 K, and then cooled in steps of 20 K back to 300 K. At each temperature, an NVT MD simulation was run for 4 ns. The present annealing temperature is above and below the melting and boiling points of ODT, 306 and 483 K, respectively. The DLPOLY package<sup>42</sup> was used to implement the MD methods described above.

A series of restrained MD simulations was run to calculate the PMF profile for the adsorption of an ODT molecule following each pathway shown in Fig. 3 in the absence of annealing. Depending on the pathway, the PMF was plotted against the horizontal position of the sulfur atom,  $\varphi$ , height of the sulfur atom,  $\xi$ , height of the methyl tail group,  $\omega$ , or both  $\xi$  and  $\omega$ . Using the umbrella sampling method,<sup>43</sup> these control variables (reaction coordinates) were restrained to their target values by imposing the harmonic bias potential functions. Typically, 39 windows were used to achieve sufficient overlaps between the neighboring histograms. For example, the target value of  $\xi$  was changed from 23.4 to 4.4 Å with a 0.5 Å decrease using a force constant of 8.0, 14.0, or 20.0 kcal (mol Å)<sup>−1</sup> for the harmonic potential functions. In each window, a 6.0 ns MD simulation was run and the initial 0.5 ns for equilibration was discarded. The free

energy was extracted using the weighted histogram analysis method.<sup>44–46</sup> At the geometries near adsorption ( $\xi < 4.4$  Å), the sulfur atom interacted strongly with the gold surface through the chemisorption potential (Morse potential). Consequently, restraining  $\xi$  to a target value became problematic. Therefore, the PMF values for the geometries very close to the adsorption of a target molecule were omitted in the PMF profiles. All of the restrained MD simulations were run using the DLPOLY combined with the PLUMED package.<sup>47</sup>

For every ODT molecule, nine united atoms of CH<sub>3</sub> or CH<sub>2</sub>, which have odd (1–17) numbers of intervening CH<sub>2</sub> groups between them and the sulfur atom, were selected. The unit vector for the tilt direction of the  $i$ th molecule,  $\vec{u}_i$ , was defined as the average over the vectors from the sulfur atom to these united atoms.<sup>33,48</sup> The tilt angle,  $\theta_i$ , was given by the polar angle of  $\vec{u}_i$  measured from the surface normal (for details, see Fig. S4, ESI†). The order parameter of the molecular orientation was defined as

$$O_u = \left\langle 0.5 \left[ (\vec{u}_i \cdot \vec{u}_j)^2 - 1 \right] \right\rangle_{i \neq j},$$

where  $\langle \rangle_{i \neq j}$  represents the average over all of the intermolecular pairs.<sup>49</sup>

## Conclusions

A nanoscale SAM of alkanethiol fabricated by contact printing inevitably features defects, where molecules are inverted among upright molecules or piled on top of the SAM. These unbound molecules can form a significant portion of a nanostructured SAM (20% in the present SAM island). Nevertheless, the molecular and thermal properties of the unbound molecules of the nanostructured SAMs were virtually unexplored, because of the inherent difficulty in the experimental probing of the nanoscale SAMs by spectroscopic or microscopic means. The present MD simulation demonstrates that thermal annealing (at 400 K) cures such defects in the SAM island of ODT that is a few nanometers in width. When heated, the SAM island slightly dispersed the sulfur atoms and alkyl chains that were densely packed. Then, the molecules piled on top of the SAM island penetrated down to make contact with the surface and the inverted molecules flipped to achieve adsorption. Upon cooling, the dense packing of the sulfur atoms and the alignment of the alkyl chains of the SAM island were recovered. We uncovered four molecular pathways behind the adsorption of unbound molecules in the annealing process. The free energy profiles for these pathways in the absence of annealing were constructed. The activation energies for these pathways were much larger than thermal energy, signifying that these unbound molecules will not be cured without the help of thermal annealing.

## Acknowledgements

This study was supported by the National Research Foundation of Korea (NRF) grant funded by the Korea government (Nos. NRF-2015R1A2A2A01004208, NRF-2014R1A4A1001690, and NRF-2012R1A6A1029029).

## Notes and references

- N. S. Pesika, F. Fan, P. C. Searson and K. J. Stebe, *J. Am. Chem. Soc.*, 2005, **127**, 11960–11962.
- R. Sahli, C. Fave, N. Raouafi, K. Boujlel, B. Schöllhorn and B. Limoges, *Langmuir*, 2013, **29**, 5360–5368.
- M. T. Dickerson, M. B. Abney, C. E. Cameron, M. Knecht, L. G. Bachas and K. W. Anderson, *Bioconjugate Chem.*, 2012, **23**, 184–195.
- N. K. Chaki and K. Vijayamohanan, *Biosens. Bioelectron.*, 2002, **17**, 1–12.
- R. Singhvi, A. Kumar, G. P. Lopez, G. N. Stephanopoulos, D. Wang, G. M. Whitesides and D. E. Ingber, *Science*, 1994, **264**, 696–698.
- M. J. Wirth, R. P. Fairbank and H. O. Fatunmbi, *Science*, 1997, **275**, 44–47.
- J. M. Tour, *Acc. Chem. Res.*, 2000, **33**, 791–804.
- F. Schreiber, *Prog. Surf. Sci.*, 2000, **65**, 151–257.
- J. C. Love, L. A. Estroff, J. K. Kriebel, R. G. Nuzzo and G. M. Whitesides, *Chem. Rev.*, 2005, **105**, 1103–1170.
- J. K. Saha, Y. Ahn, H. Kim, G. C. Schatz and J. Jang, *J. Phys. Chem. C*, 2011, **115**, 13193–13199.
- J. K. Saha, H. Kim and J. Jang, *J. Phys. Chem. C*, 2012, **116**, 25928–25933.
- H. Kim, J. K. Saha, Z. Zhang, J. Jang, M. A. Matin and J. Jang, *J. Phys. Chem. C*, 2014, **118**, 11149–11157.
- R. D. Piner, J. Zhu, F. Xu, S. Hong and C. A. Mirkin, *Science*, 1999, **283**, 661–663.
- E. Ito, J. Noh and M. Hara, *Chem. Phys. Lett.*, 2008, **462**, 209–212.
- C. Vericat, M. Vela, G. Corthey, E. Pensa, E. Cortés, M. Fonticelli, F. Ibañez, G. Benitez, P. Carro and R. Salvarezza, *RSC Adv.*, 2014, **4**, 27730–27754.
- O. Cavalleri, L. Oliveri, A. Dacca, R. Parodi and R. Rolandi, *Appl. Surf. Sci.*, 2001, **175**, 357–362.
- J.-P. Bucher, L. Santesson and K. Kern, *Langmuir*, 1994, **10**, 979–983.
- X. Xiao, B. Wang, C. Zhang, Z. Yang and M. Loy, *Surf. Sci.*, 2001, **472**, 41–50.
- N.-S. Lee, D. Kim, H. Kang, D. K. Park, S. W. Han and J. Noh, *J. Phys. Chem. C*, 2011, **115**, 5868–5874.
- C. Vericat, M. E. Vela, G. Benitez, P. Carro and R. Salvarezza, *Chem. Soc. Rev.*, 2010, **39**, 1805–1834.
- G. Gannon, J. C. Greer, J. A. Larsson and D. Thompson, *ACS Nano*, 2010, **4**, 921–932.
- S. Seo and H. Lee, *J. Phys. Chem. C*, 2011, **115**, 15480–15486.
- E. Delamarche, B. Michel, H. Kang and C. Gerber, *Langmuir*, 1994, **10**, 4103–4108.
- G. Ehrlich and F. G. Hudda, *J. Chem. Phys.*, 1966, **44**, 1039–1049.
- R. L. Schwoebel and E. J. Shipsey, *J. Appl. Phys.*, 1966, **37**, 3682–3686.
- M. Fendrich and J. Krug, *Phys. Rev. B: Condens. Matter*, 2007, **76**, 121302.
- Y. Ahn, J. K. Saha, G. C. Schatz and J. Jang, *J. Phys. Chem. C*, 2011, **115**, 10668–10674.
- J. Hautman and M. L. Klein, *J. Chem. Phys.*, 1990, **93**, 7483–7492.
- S. Krämer, R. R. Fuierer and C. B. Gorman, *Chem. Rev.*, 2003, **103**, 4367–4418.
- C. Schönenberger, J. Jorritsma, J. Sondag-Huethorst and L. Fokkink, *J. Phys. Chem.*, 1995, **99**, 3259–3271.
- M. D. Porter, T. B. Bright, D. L. Allara and C. E. Chidsey, *J. Am. Chem. Soc.*, 1987, **109**, 3559–3568.
- N. Prathima, M. Harini, N. Rai, R. Chandrashekar, K. Ayappa, S. Sampath and S. Biswas, *Langmuir*, 2005, **21**, 2364–2374.
- J. Hautman and M. L. Klein, *J. Chem. Phys.*, 1989, **91**, 4994–5001.
- P. K. Ghorai and S. C. Glotzer, *J. Phys. Chem. C*, 2007, **111**, 15857–15862.
- W. Mar and M. L. Klein, *Langmuir*, 1994, **10**, 188–196.
- J. P. Bareman and M. L. Klein, *J. Phys. Chem.*, 1990, **94**, 5202–5205.
- W. L. Jorgensen, D. S. Maxwell and J. Tirado-Rives, *J. Am. Chem. Soc.*, 1996, **118**, 11225–11236.
- W. L. Jorgensen, J. D. Madura and C. J. Swenson, *J. Am. Chem. Soc.*, 1984, **106**, 6638–6646.
- M. P. Allen and D. J. Tildesley, *Computer Simulation of Liquids*, Oxford University Press, New York, 1987.
- X. Zhao, Y. Leng and P. T. Cummings, *Langmuir*, 2006, **22**, 4116–4124.
- H. J. C. Berendsen, J. P. M. Postma, W. F. van Gunsteren, A. DiNola and J. R. Haak, *J. Chem. Phys.*, 1984, **81**, 3684–3690.
- W. Smith, C. Yong and P. Rodger, *Mol. Simul.*, 2002, **28**, 385–471.
- G. M. Torrie and J. P. Valleau, *J. Comput. Phys.*, 1977, **23**, 187–199.
- B. Roux, *Comput. Phys. Commun.*, 1995, **91**, 275–282.
- A. Grossfield, *WHAM: The Weighted Histogram Analysis Method, 2.0.8*, Grossfield Lab, Rochester, NY, 2013.
- S. Kumar, J. M. Rosenberg, D. Bouzida, R. H. Swendsen and P. A. Kollman, *J. Comput. Chem.*, 1992, **13**, 1011–1021.
- M. Bonomi, D. Branduardi, G. Bussi, C. Camilloni, D. Provasi, P. Raiteri, D. Donadio, F. Marinelli, F. Pietrucci and R. A. Broglia, *Comput. Phys. Commun.*, 2009, **180**, 1961–1972.
- R. Bhatia and B. J. Garrison, *Langmuir*, 1997, **13**, 4038–4043.
- S. Fujiwara and T. Sato, *J. Chem. Phys.*, 1999, **110**, 9757–9764.